A level-set method for analysis of microdroplet evaporation on a heated surface [†]

Gihun Son[*]

Department of Mechanical Engineering, Sogang University, Shinsu-dong, Mapo-gu, Seoul, 121-742, Korea

---

Abstract

A level-set method is presented for computing microdroplet evaporation on a heated surface. The formulation based on a sharp-interface representation for incompressible two-phase flow is extended to include the effect of evaporation by employing a calculation procedure for the coupled interface conditions for the temperature and mass fraction. A dynamic contact angle model is also incorporated into the level-set method to account for the change between advancing and receding contact angles at the liquid-gas-solid interline. The numerical method is applied to analyze the effect of wall temperature, contact angle and droplet size on the microdroplet motion.

Keywords: Conduct angle; Evaporation; Level set method; Microdroplet

---

1. Introduction

Microdroplet motion has recently attracted new attention with the development of various inkjet printing applications such as display fabrication, electronic printing, biomedical instrumentation, and micro-optics manufacturing [1]. In inkjet applications, the volatile liquid droplet ejected through a micro-nozzle acts as a carrier for the functional material to be deposited onto the target substrate. The liquid droplet is dried (or evaporated) to form a desired structure. A number of studies have been conducted to develop a predictive model for microdroplet motion that can be used to determine the design parameters in various inkjet applications. However, past efforts have suffered from the complexity of the process involving the liquid-gas interface deformed in micro-time. Further difficulties also stem from length scales, flow, temperature, and mass fraction fields influenced by the interfacial motion and the phase change coupled with heat and mass transfer.

Numerical methods for direct simulation of liquid-gas flows with phase change have been developed in several studies. For computations of the interfacial motion associated with boiling processes, Juric and Tryggvason [2] employed a front-tracking method, in which the interface is explicitly represented by the linked line or surface elements. In their method, the fluid property functions are smoothed (or smeared out) over several grid spacings. This implies that the sharp interface separating

two fluids is treated as a transition region, referred to as diffuse-interface modeling. Generally, Lagrangian methods are not straightforward for the implementation of the interface with topology change. To overcome such difficulties, Welch and Wilson [3] used the volume-of-fluid (VOF) method, which tracks the volume fraction of a particular phase rather than the interface itself. However, accurately determining the interface from the non-smooth volume-fraction function requires a complicated geometric calculation procedure [4]. Son and Dhir [5] adopted the level-set (LS) method in which the interface is tracked by a smooth distance function. Their formulation also employs diffuse-interface modeling based on smeared-out property functions, similar to those presented by Juric and Tryggvason [2]. This approach is easy to implement; however, it presents certain difficulties in accurately imposing the interface temperature condition in the diffuse-interface region where the fluid velocities are smeared out. Recently, Gibou et al. [6] and Son and Dhir [7] applied the ghost fluid approach [8, 9] based on a sharp-interface representation to film boiling on a horizontal surface and horizontal cylinder, respectively. Only a few computations have been made for evaporating liquid-gas flows coupled with mass in addition to heat transfer. Even more recently, Tanguy et al. [10] extended the LS method to droplet evaporation in air by combining it with the ghost fluid approach to account for the boundary (or matching) conditions at the liquid-gas interface for the temperature and mass fraction.

In this study, the sharp-interface LS method is further developed for computation of microdroplet motion on a heated surface. The effect of evaporation on the droplet motion is

---

included in the analysis by employing an iterative calculation procedure for the coupled interface conditions of the temperature and mass fraction. This is necessary for treating high evaporation (or mass transfer) rate problems. A dynamic contact angle model is also incorporated into the LS method to account for the change in contact angle observed during droplet evaporation on a solid surface.

2. Numerical formulation

The present numerical approach is based on the sharp-interface LS formulation developed by Son and Dhir [7] for computation of film boiling coupled with heat transfer. The LS method is extended for droplet evaporation including mass and heat transfer. Fig. 1 shows the configuration used for the analysis of an evaporating droplet on a horizontal wall. The liquid-gas interface is tracked by the LS function ϕ, which is defined as a signed distance from the interface. The negative sign is chosen for the gas phase and the positive sign for the liquid phase. In this study, we assume that the gas is an ideal mixture of air and vapor, the liquid is a pure substance, and that the interface temperature is below the saturation (or boiling) temperature.

The equations governing the conservation of mass, momentum and energy for each phase, and the vapor mass fraction Y for gas phase, are written as

$$\nabla \cdot \mathbf{u}_f = 0 \tag{1}$$

$$\rho_f(\frac{\partial \mathbf{u}_f}{\partial t} + \mathbf{u}_f \cdot \nabla \mathbf{u}_f) = -(\nabla p)_f + \rho_f \mathbf{g}$$
$$+ \nabla \cdot \mu_f (\nabla \mathbf{u} + \nabla \mathbf{u}^T)_f \tag{2}$$

$$\rho_f c_f(\frac{\partial T_f}{\partial t} + \mathbf{u}_f \cdot \nabla T_f) = \nabla \cdot k_f (\nabla T)_f \tag{3}$$

$$\rho_g(\frac{\partial Y}{\partial t} + \mathbf{u}_g \cdot \nabla Y) = \nabla \rho_g D_g \nabla Y \tag{4}$$

where the subscript "f" denotes the liquid phase ("l") for $\phi > 0$ and the gas phase ("g") for $\phi < 0$. The conservation equations for each phase are coupled through the boundary (or matching) conditions at the interface ($\phi = 0$)

$$\mathbf{u}_l - \mathbf{u}_l = v_{lg}\dot{m}\mathbf{n} \tag{5}$$

$$\mathbf{n} \cdot \left[(p_g - p_l)\mathbf{I} + \mu_l(\nabla \mathbf{u} + \nabla \mathbf{u}^T)_l - \mu_g(\nabla \mathbf{u} + \nabla \mathbf{u}^T)_g \right]$$
$$= (\sigma\kappa - v_{lg}\dot{m}^2)\mathbf{n} \tag{6}$$

$$\mathbf{n} \cdot (k_l \nabla T_l - k_g \nabla T_g) = \dot{m}h_{lg} \tag{7}$$

where $v_{lg} = \rho_g^{-1} - \rho_l^{-1}$. The normal $\mathbf{n}$ to the interface, the interface curvature κ, and the mass flux $\dot{m}$ are defined as

$$\mathbf{n} = \nabla\phi / |\nabla\phi| \tag{8}$$

$$\kappa = \nabla \cdot \mathbf{n} \tag{9}$$

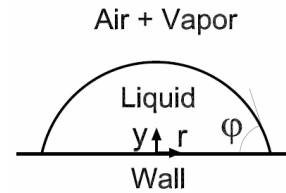$$\dot{m} = \rho_f(\mathbf{U} - \mathbf{u}_f) \cdot \mathbf{n} , \tag{10}$$

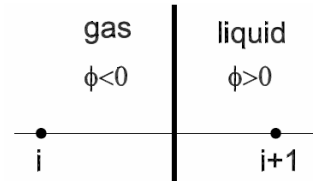Fig. 1. Configuration of an evaporating droplet on a horizontal wall.

Fig. 2. Schematic for implementation of the coupled interface conditions for the temperature and mass fraction.

where $\mathbf{U}$ is the interface velocity. The vapor mass fraction at the interface is specified as a Dirichlet boundary condition,

$$Y = Y_{\text{int}} = Y_{sat}(T_{\text{int}}) , \tag{11}$$

where Y_{int} is determined from the calculated interface temperature and the thermodynamic property relation. The mass flux $\dot{m}$ is evaluated from the mass balance at the interface,

$$\dot{m} = \frac{\mathbf{n} \cdot \rho_g D_g \nabla Y}{1 - Y_{\text{int}}} , \tag{12}$$

where Y_{int} is a function of the interface temperature, which is in turn determined to satisfy the heat flux condition given by Eq. (7). It was observed from the numerical experiments that the sequential calculation procedure of Eqs. (7), (11), and (12) for Y_{int}, T_{int} and $\dot{m}$ was not stable when coupling was strong, as in a high evaporation (or mass transfer) rate problem. As such, the three equations are combined to determine Y_{int}, T_{int} and $\dot{m}$ simultaneously as

$$\frac{\mathbf{n} \cdot \rho_g D_g \nabla Y}{1 - Y_{sat}(T_{\text{int}})} = \frac{\mathbf{n} \cdot (k_l \nabla T_l - k_g \nabla T_g)}{h_{lg}} . \tag{13}$$

Its implementation procedure is developed by considering the one-dimensional case depicted in Fig. 2. The equation is discretized as

$$\rho_g D_g \frac{Y_{sat}(T_{\text{int}}) - Y_i}{x_{\text{int}} - x_i} \frac{1}{1 - Y_{sat}(T_{\text{int}})} = \frac{k_{i+1}}{h_{lg}} \frac{T_{i+1} - T_{\text{int}}}{x_{i+1} - x_{\text{int}}} - \frac{k_i}{h_{lg}} \frac{T_{\text{int}} - T_i}{x_{\text{int}} - x_i} , \tag{14}$$

where $(x_{i+1} - x_{int})/(x_{i+1} - x_i)$ is approximated as $\phi_{i+1}/(\phi_{i+1} - \phi_i)$. When Y_i, T_i and T_{i+1} are treated explicitly, Eq. (14) is solved for the interface temperature T_{int} using a Newton-Raphson iterative algorithm. Y_{int} and $\dot{m}$ are then obtained from Eqs. (11) and (12), respectively. The mass flux $\dot{m}$ defined at the interface is extrapolated into the entire domain (or a narrow band near the interface) for its efficient implementa-

tion by the calculation procedure developed in [9].

The multidimensional implementation of Eq. (13) is accomplished in a dimension-by-dimension fashion [11] by assuming

$$\frac{\rho_g D_g \nabla Y}{1 - Y_{sat}(T_{\text{int}})} = \frac{k_l \nabla T_l - k_g \nabla T_g}{h_{lg}} . \tag{15}$$

Although Eq. (15) is not generally correct, it satisfies Eq. (13).

Based on the ghost fluid approach [6-9], a numerical technique for accurately enforcing the boundary conditions at the interface without being smoothed over several grid spacings, the conservation equations can be rewritten for the liquid-vapor region as

$$\nabla \cdot \mathbf{u} = v_{lg} \dot{m} \mathbf{n} \nabla H \tag{16}$$

$$\hat{\rho}(\frac{\partial \mathbf{u}}{\partial t} + \mathbf{u}_f \cdot \nabla \mathbf{u}_f) = -[\nabla p + (\sigma\kappa - v_{lg}\dot{m}^2)\nabla H]\hat{\rho}\mathbf{g}$$
$$+ \nabla\hat{\mu}[\nabla\mathbf{u} - v_{lg}\dot{m}\mathbf{n} + (\nabla\mathbf{u} - v_{lg}\dot{m}\mathbf{n})^T] \tag{17}$$

$$\rho_f c_f(\frac{\partial T_f}{\partial t} + \mathbf{u}_f \cdot \nabla T_f) = \nabla \cdot \hat{k}\nabla T + h_{lg}\dot{m}\mathbf{n} \cdot \nabla H \tag{18}$$

$$\rho_f(\frac{\partial Y}{\partial t} + \mathbf{u}_f \cdot \nabla Y) = \nabla \cdot \rho_f \hat{D}\nabla Y \qquad \text{if } \phi > 0$$
$$Y = Y_{sat}(T_{\text{int}}) \qquad \text{if } \phi = 0 \tag{19}$$

where

$$H = 1 \text{ if } \phi = 0$$
$$= 0 \text{ if } \phi \le 0$$
$$\mathbf{u}_l = \mathbf{u} + v_{lg}\dot{m}\mathbf{n}(1 - H)$$
$$\mathbf{u}_l = \mathbf{u} - v_{lg}\dot{m}\mathbf{n}H$$
$$\hat{\rho} = \rho_g(1 - F) + \rho_l F$$
$$\hat{\mu}^{-1} = \mu_g^{-1}(1 - F) + \mu_l^{-1}F$$
$$\hat{k}^{-1} = k_g^{-1}(1 - F) + k_l^{-1}F$$
$$\hat{D} = D_g /(1 - F) .$$

Here, H is the discontinuous step function rather than the smoothed step function varying over several grid spacings, and $\mathbf{u}_f$ ($\mathbf{u}_l$ or $\mathbf{u}_g$) is the velocity for each phase extrapolated into the entire domain by using the velocity jump condition given
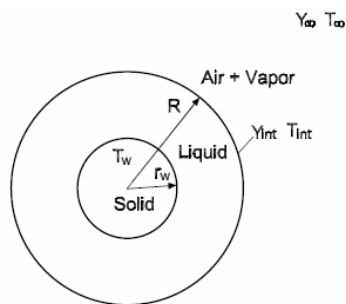
by Eq. (5). The effective (or interpolated) properties, ($\hat{\rho}, \hat{k}, \hat{\mu}$ and $\hat{D}$), are evaluated from a fraction function, F, which is defined as

$$F = 1 \text{ if } H(\phi_A) = H(\phi_B) = 1$$
$$= 0 \text{ if } H(\phi_A) = H(\phi_B) = 0$$
$$= \frac{\max(\phi_A, \phi_B)}{\max(\phi_A, \phi_B) - \min(\phi_A, \phi_B)} \qquad \text{otherwise}$$

where the subscripts A and B denote the grid points adjacent to the location where F is evaluated [7].

In the LS formulation, the interface is described as $\phi = 0$. The zero level set of ϕ is advanced as

$$\frac{\partial \phi}{\partial t} + U \cdot \nabla \phi = 0 , \tag{20}$$

where $\mathbf{U}$ can be written from Eq. (10) as $\mathbf{U} = \mathbf{u}_f + \dot{m} \mathbf{n} /\rho_f$. The LS function is reinitialized to a distance function from the interface by obtaining a steady-state solution of the equation
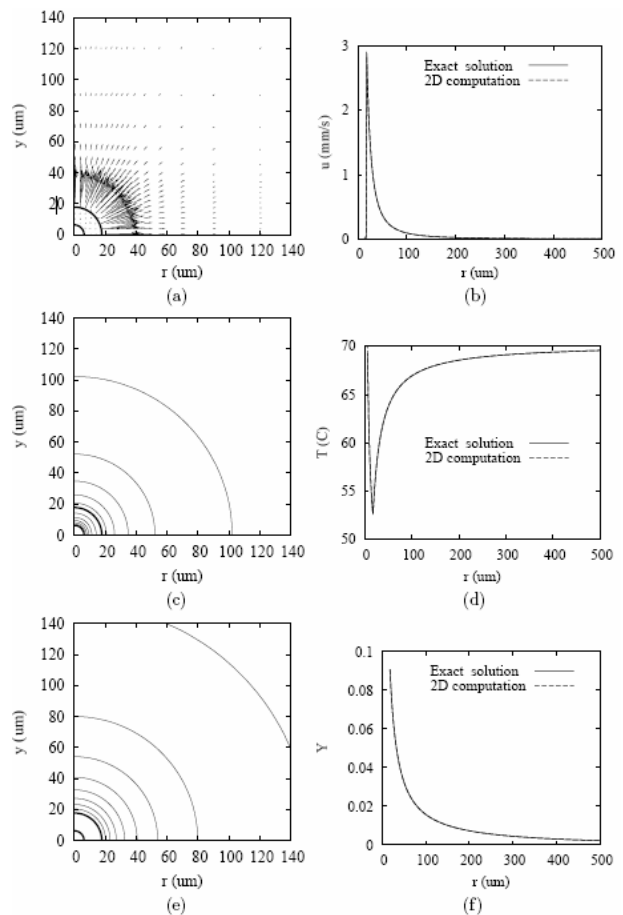

Fig. 4. Numerical results for an evaporating droplet on a spherical solid at t=21 ms: (a) velocity field; (b) velocity profile at $y = 0$; (c) temperature field; (d) temperature profile at $y = 0$; (e) vapor fraction field; and (f) vapor fraction profile at $y = 0$.

Fig. 3. Configuration of an evaporating droplet on a spherical solid.

$$\frac{\partial \phi}{\partial \tau} = S(\phi)(1 - |\nabla \phi|) , \tag{21}$$

where

$$S(\phi) = 0 \qquad \text{if } |\phi| \le h/2$$
$$= \frac{\phi}{\sqrt{\phi^2 + h^2}} \qquad \text{otherwise} \tag{22}$$

Here, h is a grid spacing. The formulation of sign function S implies that a near-zero level set rather than $\phi = 0$ is used as the immobile boundary condition during the reinitialization procedure.

In the LS formulation, a contact angle, φ, formed on the liquid-gas-solid interline can be used to evaluate the LS function at the wall [12]. The contact angle condition is expressed as

$$\mathbf{n}_w \cdot \nabla \phi = \cos\varphi , \tag{23}$$

where $\mathbf{n}_w$ is the unit normal vector pointing into the wall. The LS function at the interior node adjacent to the wall is obtained from Eq. (21). Based on typical experimental observations, the contact angle varies dynamically between an advancing (or maximum) contact angle, φ_a, and a receding (or minimum) contact angle, φ_r, as described by Fukai et al. [13]. While the interline moves, the contact angle remains constant as $\varphi = \varphi_r$ or $\varphi = \varphi_a$. However, when the interline begins to change its direction, the contact angle varies between φ_r and φ_a. In other words, the interline does not move at the wall as long as the contact angle changes in the range $\varphi_r < \varphi < \varphi_a$. Its implementation procedure is summarized as follows:

1. Assume $(\partial \phi / \partial t)_w = 0$, which means that the interline is stationary at the wall, and then evaluate a contact angle from Eq. (23), say, $\varphi = \cos^{-1}(\mathbf{n}_w \cdot \nabla \phi)$.
2. If $\varphi_r < \varphi < \varphi_a$, no further calculation is required because the interline is stationary, as assumed in Step 1. Otherwise, set $\varphi = \max \{\varphi_r, \min (\varphi_a, \varphi)\}$ since $\varphi = \varphi_r$ or $\varphi = \varphi_a$ while the interline moves.
3. Update ϕ_w from Eq. (23).

3. Numerical tests

The present numerical method is applied to water droplet evaporation in air, which is described in axisymmetric coordinates. We use the water and air properties at 1 atm: $\rho_l = 10^3 kg/m^2$, $\rho_g = 1.2\ kg/m^3$, $\mu_l = 10^{-3}\ Pas$, $\mu_g = 1.78 \times 10^{-5}\ Pas$, $k_l = 0.68\ W/mK$, $k_g = 2.48 \times 10^{-2}\ W/mK$, $D_g = 2.65 \times 10^{-5}\ m^2/s$, and $\sigma = 7.28 \times 10^{-2}\ N/m$. The saturated-vapor pressure is evaluated as a function of temperature from the steam table [14]

$$p_{v,sat} = \exp\left(9.487 - \frac{3.893 \times 10^3}{T_{int} + 230.47}\right),$$

where $p_{v,sat}$ is given in *MPa* and T_{int} in ^oC. Assuming the gas is an ideal mixture of air and water vapor, the vapor mass frac-
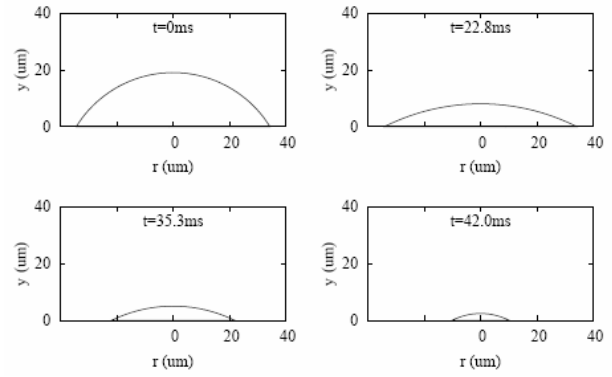

Fig. 5. Evolution of the liquid-gas interface at $D_0 = 42\mu m$, $25° \le \varphi \le 58°$ and $T_w = 70\ ^oC$.

tion is expressed at the liquid-gas interface as

$$Y_{int} = \frac{18 p_{v,sat}}{18 p_{v,sat} + 29(p_\infty - p_{v,sat})}$$

where p_∞ is the ambient pressure. The following dimensionless parameters are defined:

$$Oh = \frac{\mu_l}{\sqrt{\rho_l \sigma D_0}}, \qquad \lambda = \frac{\rho_g D_g Y_{int,0}}{\sqrt{\rho_l \sigma D_0}},$$

where the Ohnesorge number, Oh, represents the ratio of the interfacial oscillation time scale to the viscous damping time scale, and the dimensionless λ represents the ratio of the interfacial oscillation time scale to the evaporation time scale, as indicated by Lim et al. [15].

3.1 Evaporation of a spherical droplet

In this article, the LS formulation is modified to include the evaporation effect coupled with heat and mass transfer. The formulation is tested through the axisymmetric computation of droplet evaporation in a stationary air layer of infinite extent, as depicted in Fig. 3. The droplet surrounds a spherical solid whose temperature is maintained as T_w. The effect of gravity is not included in this test. Under the assumption that the droplet is always spherical, the governing equations for the conservation of mass, temperature, and vapor mass fraction are simplified as

$$\frac{1}{r^2}\frac{\partial}{\partial r} r^2 u_l = 0 \qquad \text{if } r_w < r < R$$

$$\frac{1}{r^2}\frac{\partial}{\partial r} r^2 u_g = 0 \qquad \text{if } R > r$$

$$\rho_l c_l \left(\frac{\partial T_l}{\partial t} + u_l \frac{\partial T_l}{\partial t}\right) = \frac{k_l}{r^2}\frac{\partial}{\partial r} r^2 \frac{\partial T_l}{\partial r} \qquad \text{if } r_w < r < R$$

$$\rho_g c_g \left(\frac{\partial T_g}{\partial t} + u_g \frac{\partial T_g}{\partial t}\right) = \frac{k_g}{r^2}\frac{\partial}{\partial r} r^2 \frac{\partial T_g}{\partial r} \qquad \text{if } r > R$$

$$\rho_g \left(\frac{\partial Y}{\partial t} + u_g \frac{\partial Y}{\partial r}\right) = \frac{\rho_g D_g}{r^2}\frac{\partial}{\partial r} r^2 \frac{\partial Y}{\partial r} \qquad \text{if } r > R$$
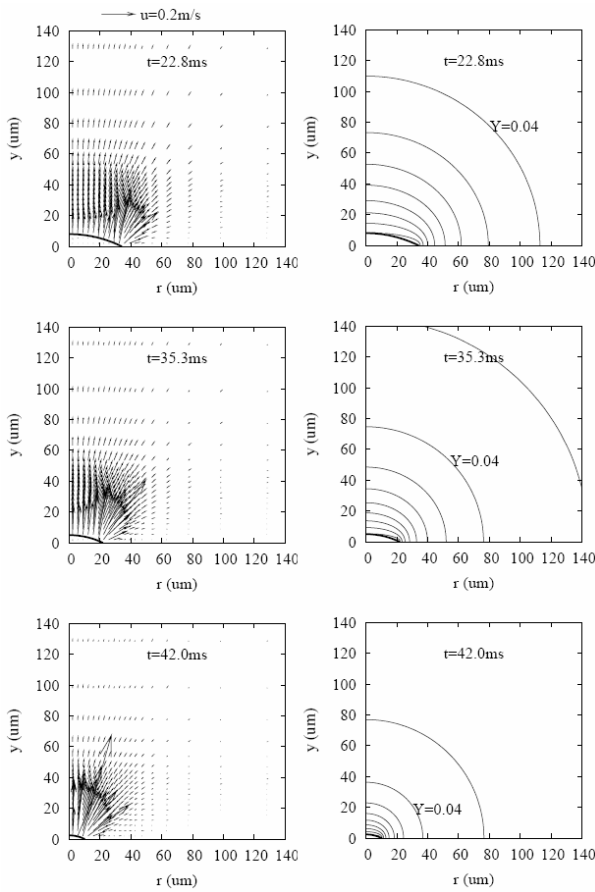
Fig. 6. Velocity and vapor fraction fields at $D_0 = 42$ μm, $25°\leq\varphi\leq58°$ and $T_w = 70$ ^oC. The interval between vapor fraction contours is 0.02.

where R is the droplet radius. The velocity profiles are easily obtained as

$$u_l = 0 \qquad u_g = -\frac{\rho_l - \rho_g}{\rho_g}\frac{R^2}{r^2}\frac{dR}{dt}.$$

To obtain near-exact temperature and mass fraction equations, we use the following coordinate transformation

$$\begin{aligned}\xi &= \frac{r - r_w}{R - r_w} && \text{if } r_w < r < R \\ &= r - R + 1 && \text{if } R > r\end{aligned}.$$

Eqs. (27)-(29) are transformed as

$$\rho_l c_l \left[\frac{\partial T_l}{\partial t} + (u_l - \xi\frac{dR}{dt})\frac{\partial T_l}{\partial t}\right] = \frac{k_l}{r^2}\frac{\partial}{\partial r}r^2\frac{\partial T_l}{\partial r} \quad \text{if } 0 < \xi < 1$$

$$\left[\frac{\partial T_g}{\partial t} + (u_g - \frac{dR}{dt})\frac{\partial T_g}{\partial t}\right] = \frac{k_g}{r^2}\frac{\partial}{\partial r}r^2\frac{\partial T_g}{\partial r} \quad \text{if } \xi > 1$$

$$\rho_g \left[\frac{\partial Y}{\partial t} + (u_g - \frac{dR}{dt})\frac{\partial Y}{\partial t}\right] = \frac{\rho_g D_g}{r^2}\frac{\partial}{\partial r}r^2\frac{\partial Y}{\partial r} \quad \text{if } \xi > 1$$

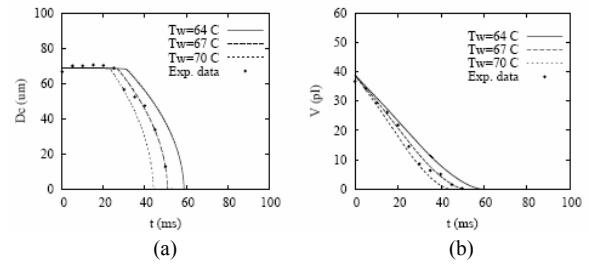This set of transformed equations is quite straightforward to discretize and solve.

Fig. 7. Effect of wall temperature on droplet motion at $D_0 = 42\mu m$ and $25°\leq\varphi\leq58°$: (a) droplet-wall contact diameter D_c and (b) droplet volume V.
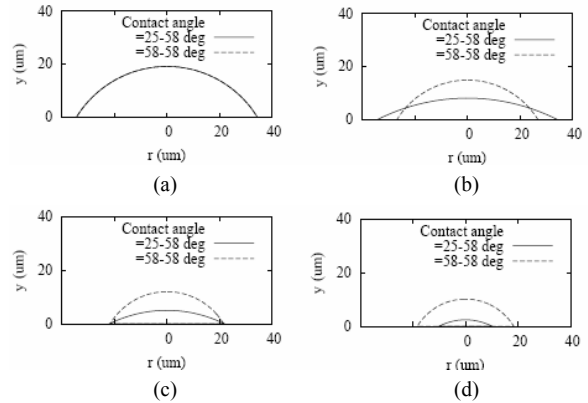

Fig. 8. Effect of dynamic contact angle on the evolution of the liquid-gas interface at $D_0 = 42$ μm and $T_w = 70$ ^oC: (a) $t = 0$ ms, (b) t = 22.8 ms, (c) $t = 35.3$ ms and (d) $t = 42.0$ ms.

The test problem is also computed using the LS formulation in cylindrical coordinates developed in this study. Initially, a spherical droplet with $R = 21$ μm is placed in a stationary air at $T = 70\,^oC$ and $Y = 0$. The droplet surrounds a spherical solid with $r_w = 6.3$ μm and $T_w = 70\,^oC$. The computational domain is chosen as a region of $r \leq 1.95\text{x}10^3$ μm and $|y| \leq 1.95\text{x}10^3$ μm. Uniform meshes with $h = 0.84$ μm are used near the droplet, $r \leq 33.6$ μm and $|y| \leq 33.6$ μm, whereas non-uniform meshes with the ratio of two adjacent intervals of 1.1 are used for the other regions to save computing time. The slip condition is imposed at the boundary of $r = 0$, while the open boundary condition is imposed at the other boundaries $r = 1.95\text{x}10^3$ μm or $|y|= 1.95\text{x}10^3$ μm. The numerical results for velocity, temperature, and mass fraction fields are plotted in Fig. 4. When compared with the almost exact (or very accurate) solutions obtained from the one-dimensional transformed equations, the predicted spatial variations of velocity, temperature and mass fraction profiles at $y = 0$ show no difference.

3.2 Droplet evaporation on a heated wall

The computations are performed for droplet evaporation on a heated wall, which is described in cylindrical coordinates, as depicted in Fig. 1. We vary the wall temperature T_w, the dynamic contact angles φ_a and φ_r, and the initial droplet diameter D_o parametrically, while keeping the ambient temperature T_∞ and vapor mass fraction Y_∞ as $25\,^oC$ and 0, respectively.
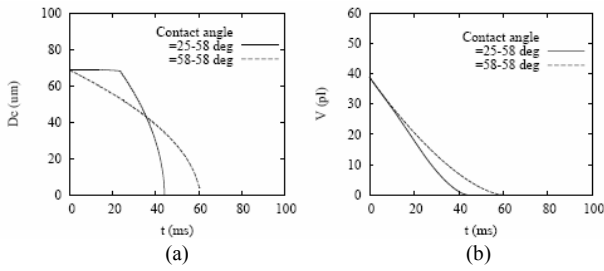
Fig. 9. Effect of dynamic contact angle on droplet motion at D_0 = 42μm and T_w = 70 ^oC: (a) droplet wall contact diameter Dc and (b) droplet volume V.
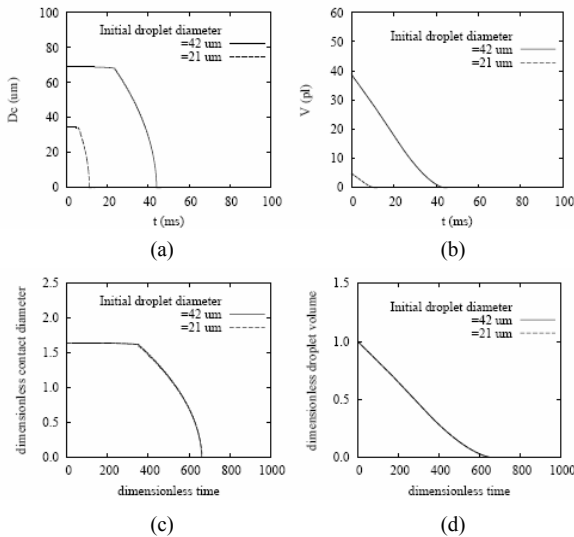

Fig. 10. Effect of droplet size on droplet motion at T_w = 70 ^oC and 25°≤φ≤58°: (a) droplet-wall contact diameter D_c; (b) dimensionless droplet-wall contact diameter D_c/D_o; and (c) dimensionless droplet volume V/V_o. The dimensionless time is defined as $D_g t/D_o^2$.

Fig. 5 shows the droplet motion at D_o = 42 μm, φ_a = 58°, φ_r = 25°, and T_w = 70 ^oC. The advancing and receding contact angles are taken from the experimental data obtained by Lim et al. [15]. Initially, the droplet shape is taken to be a spherical cap with φ = 58°, and the liquid and gas temperature to be T_w and T_∞, respectively. For t < 22.8 ms, the liquid-gas-solid interline is stationary, while the contact angle φ varies between φ_a and φ_r. After the edge of the droplet is adjusted to the receding contact angle, it moves radially inwards with $\varphi = \varphi_r$, which is consistent with the visual observation of Lim et al. [15]. The velocity and vapor fraction fields associated with the droplet motion are plotted in Fig. 6. The velocity is pronounced near the evaporating interface and decays rapidly away from the interface. The vapor fraction contours are closely packed near the droplet surface, reflecting the very high mass flux in that region.

Fig. 7 presents the effect of wall temperature on the time variations of the droplet-wall contact diameter and droplet volume. The time at which the droplet-wall contact area begins to shrink decreases with the wall temperature. Droplet life is observed to depend strongly on the wall temperature. The

results are also compared with the experimental data at T_w = 70℃ obtained by Lim et al. [15]. The numerical prediction of droplet behavior is comparable to the experimental data except that the corresponding wall temperature is slightly mismatched.

Figs. 8 and 9 show the dependence of droplet motion on the receding contact angle φ_r. The evaporation rate is found to increase as φ_r decreases. This is expected because with the reduction of the receding contact angle the liquid-gas interface area increases and the averaged distance between the interface and the heated wall decreases, as seen from Fig. 8.

The droplet motions for two different droplet sizes of D_o = 42 μm and D_o = 21 μm are compared in Fig. 10. The droplet evaporation rate and droplet lifetime are very different for both cases. However, when the droplet characteristics are scaled by the initial droplet diameter D_o and the mass diffusivity D_g, the dimensionless curves for both droplet sizes overlap. This indicates that the microdroplet evaporation process is controlled by the diffusion effect rather than the convection effect, and the surface tension has little influence on droplet evaporation as long as the dimensionless parameter λ is small.

4. Conclusions

A level-set method was developed for simulating microdroplet evaporation on a heated surface. The formulation based on a sharp-interface representation for incompressible two-phase flows was extended to include the effect of evaporation at the liquid-gas interface by employing a calculation procedure for the coupled interface conditions of the temperature and mass fraction. In addition, a dynamic contact angle model was incorporated into the method to account for the change between advancing and receding contact angles at the liquid-gas-solid interline. The numerical prediction of droplet motion is observed to be comparable to the exact solution or the experimental data available in the literature. The method was proven applicable to investigating the effects of wall temperature, dynamic contact angle, and droplet size on the microdroplet motion.

Acknowledgment

References

[1] J. Berthier, *Microdrops and Digital Microfluidics*, William Andrew, (2008).

[2] D. Juric and G. Tryggvason, Computations of boiling flows, *Int. J. Multiphase flow*, 24 (1998) 387-410.

[3] S. W. J. Welch and J. Wilson, A volume of fluid based method for fluid flows with phase change, *J. Comput. Phys.*, 160 (2000) 662-682.

[4] W. J. Rider and D. B. Kothe, Reconstructing volume track-

ing, *J. Comput.Phys.,* 141 (1997) 112-152.

[5] G. Son and V. K. Dhir, Numerical simulation of film boiling near critical pressures with a level set method, *J. Heat Transfer*, 120 (1998) 183-192.

[6] F. Gibou, L. Chen, D. Nguyen and S. Banerjee, A level set based sharp interface method for the multiphase incompressible Navier-Stokes equations with phase change, *J. Comput. Phys.*, 222 (2007) 536-555.

[7] G. Son and V. K. Dhir, A level set method for analysis of film boiling on an immersed solid surface, *Numer. Heat Transfer B*, 52 (2007) 153-177.

[8] D. Q. Nguyen, R. P. Fedkiw and M. Kang, A boundary condition capturing method for incompressible flame discontinuities, *J. Comput. Phys.*, 172 (2001) 71-98.

[9] F. Gibou, R. P. Fedkiw, L.-T. Cheng and M. Kang, A second-order-accurate symmetric discretization of the Poisson equation on irregular domains, *J Comput. Phys.*, 176 (2002) 205-227.

[10] S. Tanguy, T. Menard and A. Berlemont, A level set method for vaporizing two-phase flows, *J. Comput. Phys.*, 221 (2007) 837-853.

[11] S. Osher and R. Fedkiw, *Level Set Methods and Dynamics Implicit Surfaces*, Springer-Verlag, New York, (2003).

[12] Y. Suh and G. Son, A sharp-interface level-set method for simulation of a piezoelectric inkjet process, *Numer. Heat Transfer B*, 55 (2009) 295-312.

[13] J. Fukai, Y. Shiiba, T. Yamamoto, O. Miyatake, O. Poulikakos, C. M. Megaridis and Z. Zhao, Wetting effects on the spreading of a liquid droplet colliding with a flat surface, *Phys. Fluids*, 7 (1995) 236-247.

[14] F. I. Jr. Thomas and E. L. Peter, *Steam and Gas Tables with Computer Equations*, Academic Press, (1984).

[15] T. Lim, S. Han, J. Chung, J. T. Chung, S. Ko and C. P. Grigoropoulos, Experimental study on spreading and evaporation of inkjet printed pico-liter droplet on a heated substrate, *Int. J. Heat Mass Transfer*, 52 (2009) 431-441.

Gihun Son received his B.S. and M.S. degrees in Mechanical Engineering from Seoul National University in 1986 and 1988, respectively, and his Ph.D. degree in Mechanical Engineering from UCLA in 1996. Dr. Son is currently a professor of Mechanical Engineering at Sogang University in Seoul, Korea. His research interests are in the areas of multiphase dynamics, heat transfer, and power system simulation.